Bulletin of the Seismological Society of America, Vol. 100, No. 6, pp. 3304–3311, December 2010, doi: 10.1785/0120100051

Short Note

Crustal Structure below the Valley of Mexico Estimated from Receiver Functions

by V. M. Cruz-Atienza, A. Iglesias, J. F. Pacheco, N. M. Shapiro, and S. K. Singh

Abstract Receiver functions (RFs) from two permanent stations (CUIG and ZAIG) of the Mexican broadband network were calculated to infer the crustal structure at both sites. The data were stacked to allow uncertainty estimations and inverted using two global optimization algorithms: simulated annealing and genetic algorithms. Strong and systematic azimuthal dependence was observed in the stacked functions at CUIG site, which is located in the Mexican volcanic belt (MVB). Assuming a one-dimensional five-layer model per azimuthal stack, these variations were explained with the same upper crustal structure including a superficial ~2 km-thick low-velocity layer associated with the MVB and a well-defined Conrad interface around 15 km depth, different depths for the Moho discontinuity, and variations in both the *S*-wave velocity and Poisson's ratio for the upper mantle. Our inversion of observed RFs at CUIG and theoretical considerations suggest an eastward crustal thickening of at least 5 km below the Valley of Mexico. We tested the sensitivity of the modeling procedure by applying it to the recordings at ZAIG station. In this case, no azimuthal dependence was noticed in the stacked functions. After a simultaneous inversion of three different azimuthal stacks, a single four-layer model satisfactorily explained all data, thus revealing a flat one-dimensional crustal model below the Mexican Mesa Central, where ZAIG station is located. These results support the resolution and robustness of the applied method at both sites.

Introduction

Path effects like multipathing and regional amplification may play a very important role for seismic hazard in Mexico City during large earthquakes in the Mexican subduction zone (e.g., Singh *et al.*, 1988; Campillo *et al.*, 1989). For this reason, many studies have been devoted to obtaining better knowledge of the crustal structure in central Mexico, including inversion of surface-wave dispersion curves (Gomberg *et al.*, 1988; Campillo *et al.*, 1996; Shapiro *et al.*, 1997; Iglesias *et al.*, 2001; Rivet *et al.*, 2009; Iglesias *et al.*, 2010), ray tracing (Valdés-Gonzáles and Mayer, 1996), teleseismic tomography (Gorbatov and Fukao, 2005; Husker and Davis, 2009), gravity modeling (Urrutia-Fucugauchi and Flores-Ruíz, 1996), and magnetotelluric analysis (Jodicke *et al.*, 2006). Most of these studies, while providing information about average crustal properties, do not well-resolve the depth of the Moho and crustal discontinuities.

The receiver function (RF) technique (Langston, 1979) allows an estimation of higher-resolution crustal models below the recording stations. It has been used to estimate the Mexican crustal structure below individual stations located in regions with remarkably different geological settings (e.g., Cruz-Atienza *et al.*, 1998; Cruz-Atienza, 2000; Cruz-Atienza *et al.*, 2001; Persaud *et al.*, 2007; Obrebski and Castro Escamilla, 2008; Espindola Castro, 2009). More recently, Pérez-Campos *et al.* (2008) and Greene-Gondi (2009) applied the RF technique to image the subducting Cocos plate under the North American plate along a 400-km-long seismic profile crossing the Valley of Mexico. Their results suggest that the deep lithospheric structure under the valley is strongly affected by both the detachment of the subducting slab from the upper plate and the mantle wedge. This observation seems to be supported by teleseimic *P*-wave tomography using the same data (Husker and Davis, 2009). However, because the RFs technique used by these authors assumes a one-dimensional structure to migrate the arrival times of converted phases over a two-dimensional vertical projection, their results may not resolve the structure geometry in highly heterogeneous media. As a result, inferred geometry of the interfaces below the Valley of Mexico may be significantly biased.

In order to find a well-constrained crustal model beneath the Valley of Mexico, we applied an RF inversion technique

(Cruz-Atienza, 2000; Cruz-Atienza *et al.*, 2001) using stacked *P*-wave forms from teleseismic events recorded at the broadband station CUIG, which is located within Mexico City in the Mexican volcanic belt (MVB; Fig. 1). Teleseismic *P* waves arrive almost vertically at CUIG station, allowing a complete mapping of the crust from converted phases at strong interfaces. The crustal models are obtained from the inversion of stacked waveforms and their uncertainties using two global optimization methods: genetic algorithms (GA) and simulated annealing (SA) algorithms.

Because of the strong azimuthal dependence observed in the stacked functions over the MVB, we tested the methodology by applying it to records obtained at station ZAIG, further north from Mexico City, where no such relevant dependence was noticed. This station is located in the city of Zacatecas, Mexico, above the Mexican Mesa Central (MC) geologic province (Nieto-Samaniego *et al.*, 1999), close to the eastern edge of the Sierra Madre Occidental (SMOc, Figure 1). The same simple model could satisfactorily predict the stacked functions from three different azimuths. In contrast, due to the strong azimuthal variations of the RFs at the CUIG site, we found significant changes in the deep structure around that station. Results from the two geological provinces confirm that the applied methodologies have enough resolution and the observed differences are real.

Data and Inverse Problem

An RF could be simply defined as a time series that contains the entire shear-wave field converted at the layered structure that lies below the station. These series are obtained by a deconvolution between the radial (or transversal) and the vertical components of the recorded seismograms. Langston (1979), Owens *et al.* (1984), and Ammon (1991) broadly describe the supporting theory for this technique. The two stations that were used to obtain the observed RFs, CUIG and ZAIG (Fig. 1), belong to the Mexican seismic network of the Servicio Sismológico Nacional. Each one has an STS2 broadband seismometer connected to a Quanterra 24-bit digitizer. For all data, we applied a low-pass Gaussian filter with a cut-off frequency at 0.33 Hz and a water-level between 0.005–0.05 for achieving stability during the deconvolution processes carried out in the frequency domain. The epicentral distance of all teleseismic events ranges between 30 and 90 degrees. Records at both stations were classified according to the azimuth from which they come. We thus define four clusters (i.e., groups) of events in the case of CUIG station (triangles, Fig. 1) and three for ZAIG station (circles, Fig. 1). RFs for each cluster were stacked to reduce noise. This procedure also allowed us to estimate uncertainties from the data, generating a standard deviation band around the average of the stacked functions (dotted lines in Fig. 2b and Fig. 3b; and dashed lines in Fig. 4) with surface $S_b = 2\int_0^T \sigma(t)dt$, where $\sigma(t)$ is the time-dependent standard deviation function and T the duration of the RF time window. As detailed later, this error band was used to select the whole of model solutions that correspond to the data uncertainty.

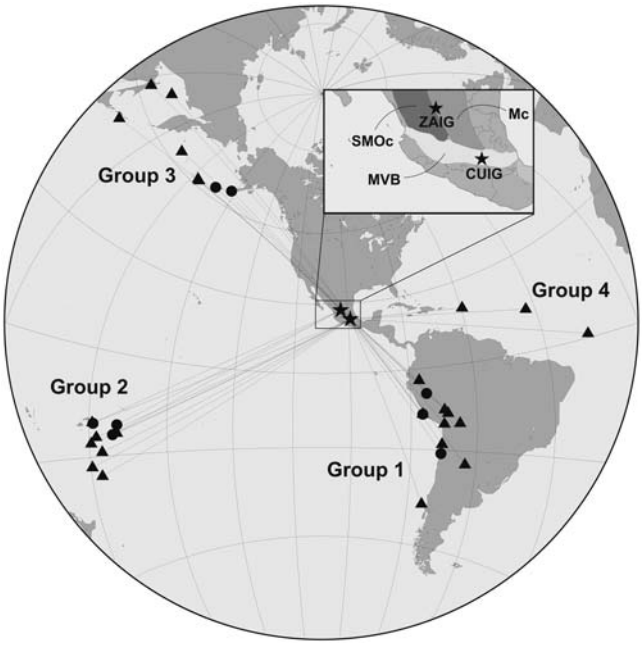

Figure 1. Stations and epicenters locations. Solid circles, events recorded at ZAIG station; black triangles, CUIG station; groups 1–4, azimuthal groups associated with each station. Inset: Sierra Madre Occidental (SMOc), Mesa Central (Mc), and Mexican volcanic belt (MVB) geological provinces.

To invert the observations we employed two global optimization methods: genetic algorithms (Holland, 1975; Goldberg, 1989) and simulated annealing (Metropolis *et al.*, 1953; Kirkpatrick *et al.*, 1983). Iglesias *et al.* (2001) discuss a detailed description of the specific algorithms used in our inversions, including several improvements. Both methods search for solutions in the same model space for each station, achieving almost the same results. We used these two algorithms to make sure they converge to the same solutions and hence to further validate our final conclusions. The initial models parameterization was built from all available information for both regions from previous works. Both thickness and shear-wave velocities of one-dimensional stratified media were inverted simultaneously.

The simple and similar shapes of radial RFs at ZAIG (Fig. 3b) suggested a simple four-layer crustal model, similar to that proposed by Nieto-Samaniego *et al.* (1999). Taking this into account, the model space was established (dashed lines, Fig. 3a) and a simultaneous inversion of the three stacked functions could be carried out for this site. In order to parameterize the inverse problem in the case of CUIG, we integrated two previous models: (1) the one first introduced by Havskov and Singh (1977–78) from refraction seismology and latter confirmed by Shapiro *et al.* (1997) from Rayleigh-wave dispersion-curve analysis, consisting of an uppermost low *S*-wave velocity layer associated with both volcanic deposits and volcanic activity along the southern part of the MVB; and (2) the regional crustal model proposed

by Campillo *et al.* (1996), which represents an averaged velocity structure from Guerrero's coast to the Valley of Mexico determined from the inversion of surface-waves dispersion curves. Thus, the reference model at CUIG, from which the model space was established (i.e., lower and upper limits for the inverted parameters; dashed lines, Fig. 2a), consists of a five-layer velocity structure. As we shall see, due to important differences between the four stacked RFs (Fig. 2b and Fig. 4), it was necessary to solve the inverse problem individually per cluster.

While we assumed a Poissonian solid (i.e., $\nu = 0.25$, which implies $V_P = \sqrt{3}V_S$, where V_S and V_P are the *S*-wave and *P*-wave velocities, respectively) for the inversion at ZAIG, the Poisson's ratio for the crust beneath CUIG was fixed using the P − Ps and P − PpPms delay technique described by Zandt and Ammon (1995). The value we found ($\nu = 0.275$), which is slightly higher than that of a Poissonian solid, is in agreement with the range reported for the Mexican crust by Zandt and Ammon (1995) and Campillo *et al.* (1996). Because of the active volcanism within the MVB and close to Mexico City (e.g., the Popocatépetl volcano; see Shapiro *et al.*, 2000), the upper-mantle Poisson's ratio was also inverted at the CUIG site. At both sites and for all inversions, we assume the density to be given by the formula $\rho = 0.32\ V_P + 0.77$ (Berteussen, 1977).

We applied one criterion with two conditions to select solution models. The first condition was that every solution model must have a misfit function smaller than a given threshold value. The misfit function is the semblance between the observed and the synthetic curves, which is defined as

$$E(m_c) = 0.5 - \frac{\text{cross}(d_s, d_o)}{\text{auto}(d_s) + \text{auto}(d_o)},$$

where $E(m_c)$ is the semblance of the current model m_c, $\text{auto}(d_s)$ and $\text{auto}(d_0)$ are the autocorrelation of the synthetic and observed data, respectively, and $\text{cross}(d_s, d_o)$ is the cross correlation of both signals. The second condition required that the synthetic RF from a solution model must lie as much as possible within the error band mentioned earlier. To this purpose, we define the relative area of the synthetic RF outside the error band with respect to S_b as

$$S_R(m_c) = \frac{100}{S_b}\int_0^T g(t)dt$$

$$\text{where } g(t) = \begin{cases} |d_s - d_o| - \sigma & ; \quad t \ni \sigma \le |d_s - d_o| \\ 0 & ; \quad t \ni \sigma > |d_s - d_o| \end{cases}.$$

The selection criteria thus impose both that S_R is smaller than 15% and that the misfit function E is smaller than 0.1. Two thousand final models, 1000 from GA and 1000 from SA, were selected this way for each inversion. They are presented together in Figure 2a and Figure 3a.

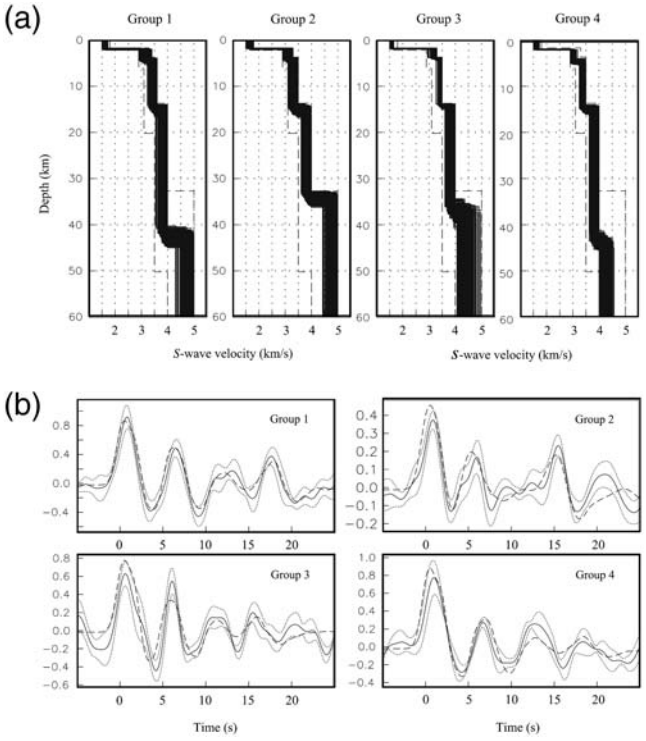

Figure 2. a) Two thousand solution models yielded by the independent inversions of the four stacked RFs at CUIG site (solid lines), with bounds of the model space in which the two global optimization methods searched for the solution models (dashed lines). b) Comparison between the stacked RFs (solid lines) with their error bands given by the standard deviation of the averaged functions (dotted lines) and the synthetic RF from each average solution model (dashed lines).

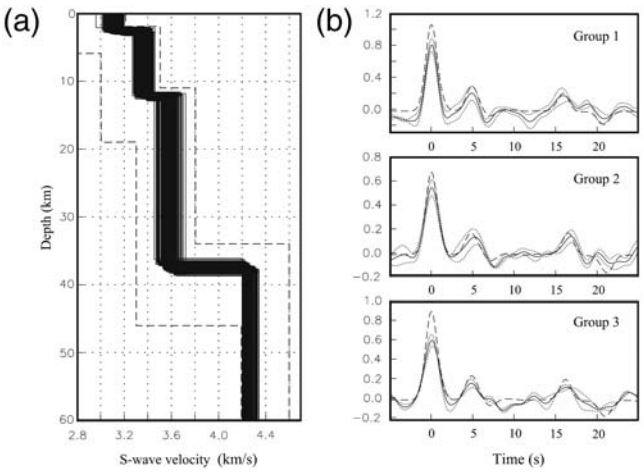

Figure 3. a) Two thousand solution models obtained by the simultaneous inversion of the three stacked RFs on the ZAIG site (solid lines) with bounds of the model space in which the two global optimization methods searched for the solution (dashed lines). b) Comparison between the stacked RFs at ZAIG station (solid lines) with their error bands given by the standard deviation of the averaged functions (dotted lines) and synthetic RFs from the average solution model (dashed lines).

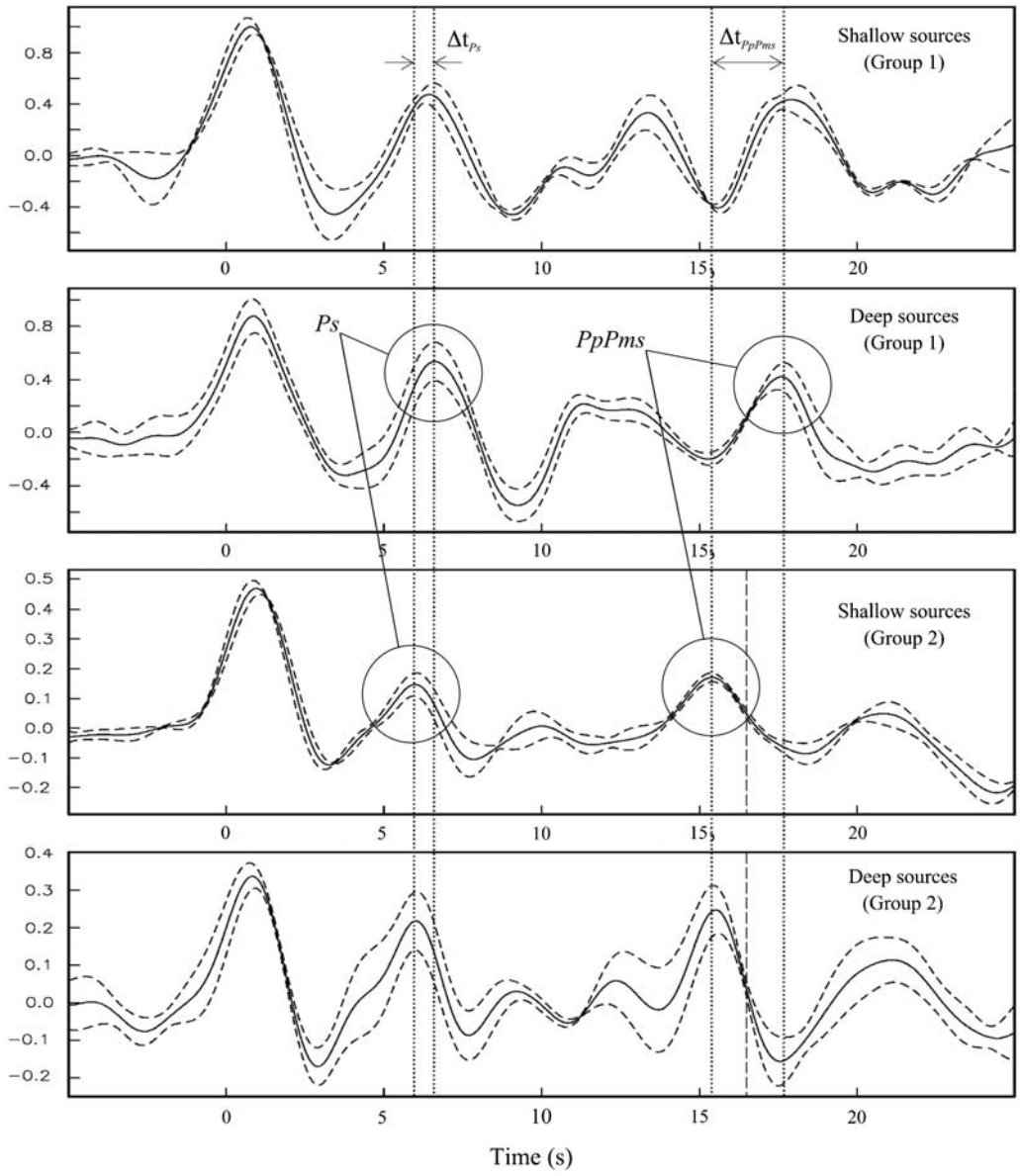

Figure 4. Stacked RFs for groups 1 and 2 separated into two subgroups, one for shallow and the other for deep hypocentral locations (solid lines) along with their standard deviation bands (dashed lines). Arrival times (long vertical dashed lines) and waveforms of the Ps and the PpPms phases (circles) for each group are indicated. Theoretical arrival time of the PpPms phase for a flat Moho below the Valley of Mexico in the observed RF from group 2 is indicated by a short vertical dashed line (see text).

Modeling Results

The 2000 solution models per stack yielded by our inversions at CUIG station are presented in Figure 2a (solid lines). Table 1 reports the corresponding numerical values with their standard deviations for all model parameters. Synthetic RFs from the average solution models for each inversion are compared with data in Figure 2b (dashed lines). Very similar crustal models were obtained from the four independent inversions. The superficial low-velocity layer associated with volcanic deposits and the active volcanism in the MVB was essential to achieve such fits. The standard deviations (uncertainties) yielded by the inversion results for that layer are smaller than 20% of the ranges of variability set for both associated parameters (i.e., layer thickness and V_S), revealing a strong sensitivity of our inverse problem to the presence of such an uppermost geologic unit. Moreover, the depth of the Conrad discontinuity around 15 km coincides remarkably well for all groups. In contrast, significant variations were required in the deep crustal structure to fit the observed RFs. These variations concern both the Moho's elastic contrast and depth (see Figure 2a and Table 1). Results reveal an interesting spatial correlation between high Poisson's-ratio (ν) values for the upper mantle (i.e., models for groups 2

and 4 relative to those for groups 1 and 3) and the east–west-trending direction of active volcanism along the southernmost edge of the MVB, where the Popocatépetl and other volcanoes are located. Notice that the highest ν value and lowest S-wave velocity for the upper mantle correspond to the crustal model of group 4 ($\nu = 0.295$ and $V_S = 4.23$ km/s), for which the PpPms phase enters the crust about 10 km to the north of the Popocatépetl active volcano (see Cruz-Atienza, 2000). This result is in agreement with previous and independent estimates (Cruz-Atienza *et al.*, 2001).

By simply inspecting our data, the stacked functions at the CUIG site reveal important differences between the four averaged curves (Fig. 2b). Most relevant differences consist in arrival times and amplitudes of the PpPms Moho reverberation phases (around 14–18 s), which considerably differ in the stacks for groups 1 and 4, in comparison with those for groups 2 and 3. A smaller delay on the Ps Moho converted phases (around 5–7 s) can also be noticed. To assess the robustness of such striking observation and to elucidate if it is a consequence of source location, we separated the RFs for groups 1 and 2 (those with more available data) into two subgroups, one for shallow and the other for deep hypocenter locations. Average hypocentral depths for subgroups from group 1 are 43 ± 32 km and 615 ± 29 km, while those from group 2 are 58 ± 46 km and 563 ± 23 km. Figure 4 presents the stacked RFs per subgroup (solid lines) along with their standard deviation bands (dashed lines). Arrivals of the Ps and the PpPms phases mentioned earlier are indicated with circles. This figure reveals two relevant matters concerning such phases: (1) consistency in the arrivals' waveforms in all cases is larger than 75% of their average value, and (2) no matter the hypocentral depth, both the Ps and the PpPms arrival times for each group (vertical dotted lines) are consistent with each other and significantly different between both azimuthal groups.

The observed arrival times for these phases give differences $\Delta t = t_{PpPms} - t_{Ps}$ equal to 11.2 s and 9.5 s, respectively, for groups 1 and 2. The ratio between them, $\Delta t_R = \Delta t_2/\Delta t_1 = 0.85$, directly depends on both the teleseimic P-wave incidence angle at the Moho and the crustal thickness below the wave propagation region for each azimuthal group. Simple geometrical considerations lead us to formulate an expression for that time-delay ratio due to waves propagating throughout two crustal models with different thicknesses, h_1 and h_2, as $\Delta t_R = (h_2/h_1)(\cos\gamma_{P1}/\cos\gamma_{P2})$. In this expression, γ_{P1} and γ_{P2} are the P-wave transmission angles at the Moho discontinuity for each model. On the other hand, the average incidence angles of teleseimic P waves at the Moho below CUIG site are 32° and 19°, respectively, from groups 1 and 2. Thus, by taking both the upper mantle P-wave velocities and Poisson's ratios given by our final models for these groups (Table 1), an average P-wave crustal velocity equal to 6.1 km/s, and the observed $\Delta t_R = 0.85$, we get a theoretical crustal thickness ratio $h_2/h_1 = 0.89$. Assuming the Moho depth obtained from group 1 to be correct (i.e., $h_1 = 42.7$ km), then the observed time-delay ratio requires the crustal thickness along the group 2 azimuthal path to be $h_2 = 38$ km. Compared with the maximum Moho depth yielded by the inversion for that group (35.3 km), our theoretical prediction is slightly greater (i.e., 2.7 km higher). However, if the crustal thickness along both azimuthal paths were the same (i.e., $h_2/h_1 = 1.0$), then we would expect $\Delta t_R = 0.95$ from the data. In that hypothetical case, the PpPms arrival time for group 2 should be around 16.5 s (see dashed vertical lines inside panels for group 2 in Fig. 4), which is about 1.2 s later than the actual arrival time. Thus, an eastward crustal thickening of about 5 km is suggested directly from our data.

To better assess the structural agent causing the observed arrival-time delay below the MVB, we computed transverse RFs at station CUIG (see Cruz-Atienza, 2000). Unfortunately, the lack of good azimuthal coverage made it impossible to identify systematic features revealing, for example, the presence of dipping interfaces (Cassidy, 1992). Several attempts to simultaneously invert the four radial stacks failed because satisfactory fits to the data could not be obtained. The only way to explain these differences in the observed data was to allow variations in the Moho's depth and in both the shear-wave velocities and Poisson's ratios in the upper mantle at individual inversion processes for each cluster.

In order to assess the reliability of the deep structure variations beneath the MVB suggested by our final models, we applied the same methodology to the data recovered at ZAIG station, where no strong azimuthal dependence is present (Fig. 3b). In this case, the simultaneous inversion of three stacks from groups 1, 2, and 3 was possible. Thus, every selected model could simultaneously satisfy the six conditions, two per stack, imposed by the inversion algorithms. The 2000 model solutions are shown in Figure 3a (solid lines), and the synthetic RFs from the average solution model are compared with data in Figure 3b (dashed lines). In agreement with previous studies (Nieto-Samaniego *et al.*, 1999), a simple four-layer model could satisfactorily explain the three stacked functions. Therefore, an approximately one-dimensional layered crust exists below Zacatecas. These results also confirm that, when a one-dimensional model is assumed per RF inversion, the strong azimuthal variations seen in our RFs at the CUIG site may only be explained by significant lateral changes in the deep crustal structure (i.e., Moho depths and elastic contrasts).

Discussion and Conclusions

Stacked RFs upon the MVB at the CUIG site present a strong and consistent azimuthal variation. Independent global inversions for each azimuthal stack explained all data remarkably well. The set of 2000 solution models selected by two independent inversion algorithms reveals the upper and middle crustal structures to be essentially the same in all azimuthal directions. Solution models consist of a five-layer crustal structure with a low-velocity ~2 km-thick uppermost layer, which characterizes the southern part of the MVB

Table 1
Numerical Values for the Average Solution Models Obtained from the Four Independent Inversions at CUIG Site*

Group	Parameter	Layer 1	Layer 2	Layer 3	Layer 4	Layer 5
1	V_S (km/s)	1.55 ± 0.038	3.14 ± 0.128	3.50 ± 0.070	3.88 ± 0.086	4.80 ± 0.121
	h (km)	1.97 ± 0.094	2.34 ± 0.285	10.79 ± 0.568	27.62 ± 0.979	∞
2	V_S (km/s)	1.59 ± 0.069	3.16 ± 0.095	3.31 ± 0.090	3.79 ± 0.077	4.78 ± 0.131
	h (km)	1.81 ± 0.077	2.39 ± 0.287	10.66 ± 0.588	19.21 ± 0.274	∞
3	V_S (km/s)	1.52 ± 0.016	3.25 ± 0.053	3.47 ± 0.025	3.88 ± 0.068	4.37 ± 0.147
	h (km)	1.84 ± 0.034	2.08 ± 0.081	10.17 ± 0.143	23.08 ± 0.817	∞
4	V_S (km/s)	1.58 ± 0.044	2.96 ± 0.054	3.42 ± 0.048	3.88 ± 0.063	4.23 ± 0.102
	h (km)	2.08 ± 0.064	2.39 ± 0.247	10.38 ± 0.337	28.78 ± 0.680	∞

*See Figure 2a. V_S is the *S*-wave velocity and h the layer thickness. Numerical values obtained for the upper-mantle (layer 5) Poisson's ratio (ν) are 0.273 ± 0.008, 0.290 ± 0.005, 0.269 ± 0.039, and 0.295 ± 0.005, respectively for groups 1–4. The corresponding value for the crust (i.e., for layers 1–4) was constant and equal to $\nu = 0.275$.

province where active volcanism is present. This superficial layer has been identified from boreholes as a heterogeneous geologic unit consisting of a series of andesites and volcanic tuffs intermixed with sands, shales, sandstones, lacustrine limestones, breccias, and conglomerates (Marsal and Graue, 1969). Below a ~4.5 km depth impedance interface, we found a consistent and very well defined Conrad discontinuity at ~15 km depth. *S*-wave velocities within the lower crust (i.e., below the Conrad discontinuity) are also consistent around 3.9 km/s. However, our inversions revealed significant lateral changes in the deep structure regarding the Moho's depth and both the *S*-wave velocities and Poisson's ratios in the upper mantle. By considering the estimated uncertainty in our final models, the highest difference in the Moho depth was found to be about 7 km between models from group 2 (to the west of the station) and group 4 (to the east). Taking the places where the corresponding PpPms phases enter the crust per group, such difference in depth occurs over an ~80 km-long east–west-trending region, which implies an eastward crustal thickening with a Moho slope of about 9%. Similar Moho depth variations have been inferred using RF analysis in different worldwide regions (e.g., Bertrand *et al.*, 2002; Yuan *et al.*, 2002; Lombardi *et al.*, 2008). In accordance with a previous and independent study (Cruz-Atienza *et al.*, 2001), our results also show that, below the very high and active Popocatépetl volcano, we have (1) the deepest crustal root and (2) both the slowest *S*-wave velocity (~4.2 km/s) and highest Poisson's ratio (~0.29) in the upper mantle. These results seem to be correlated with the active volcanism that rises from the mantle below this specific region of the MVB. Crustal thickening there has also been recently identified with surface-wave tomography by Iglesias *et al.* (2010). They infer an even steeper Moho discontinuity along a north–northeast vertical cross section, suggesting a crustal thickening of nearly 10 km over a horizontal distance of 60 km.

Detailed inspection of the data from groups 1 and 2 lead us to theoretical considerations showing that, if the eastward crustal thickening does not exist (i.e., if the Moho's depth was the same in both azimuthal directions), then the PpPms phase, clearly identified in the observed RFs, should arrive at the station ~1.2 s later than it appears in the stacks for group 2. Such time delay represents about 25% of the *P*-wave travel time to traverse the crust. This analysis, which is independent from the inversion results, supports the same conclusion suggested by our final structural models regarding the crustal thickening from west to east below the Valley of Mexico.

Using a simple model of isostatic compensation due to topographic loading, we can estimate the difference in the Moho's depth between two adjacent (uncoupled) crustal regions with dissimilar average elevations as $\Delta M_{\text{depth}} = (1/C - 1)\Delta_{\text{topo}}$. In this equation, Δ_{topo} is the difference of topographic elevation between the two regions, $C = 1 - (\rho_c/\rho_m)$, and ρ_c and ρ_m are the average densities of the crust and mantle, respectively. Considering Δ_{topo} between the eastern high-elevation volcanic region and the much lower west–northwest border of the Valley of Mexico ranging between 1200 and 1700 m and assuming the crustal and mantle densities as 2750 and 3300 kg/m^3, respectively, we have $\Delta M_{\text{depth}} = 7.3 \pm 1.3$ km. This estimate, which is in agreement with the one reported previously as yielded by our RF inversions, represents the third independent result supporting the idea of an eastward crustal thickening below the valley.

Applying the same inverse modeling methodology to the stacked RFs at the ZAIG site for three different azimuthal regions, the same simple four-layer one-dimensional model satisfactorily explained all data. Except for the low-velocity superficial layer associated with the MVB at the CUIG site, the upper-crustal structures (those above the Conrad discontinuity) determined in both sites are remarkably similar in terms of wave propagation speeds: two layers with average *S*-wave velocities of 3.18 and 3.37 km/s from the surface to the interior at ZAIG site (compare with Table 1). Upper-crust structural differences between both geological provinces arise in the depths of the interfaces, being more superficial below the MC province and equal to 2.9 km for the first interface and 12 km for Conrad discontinuities. Velocities in both

the lower crust and upper mantle are relatively low there, with average values of 3.56 and 4.23 km/s, respectively. Below the western edge of the altiplano region where the ZAIG site is located (i.e., very close to the SMOc mountain range province), we found the Moho to be 37.4-km depth on average, which is very close to the depth determined for the west–northwest regions of the Valley of Mexico (groups 2 and 3, Table 1). Inversion results obtained at the ZAIG site, where no azimuthal dependence in the RFs was observed, provide confidence in the resolution and robustness of the applied modeling methodology that proved to be very sensitive to variations observed in the stacked functions at the CUIG site.

Data and Resources

Seismograms used in this study were provided by the National Seismological Network belonging to the Mexican Servicio Sismológico Nacional (SSN). (For access and permission to use the data, the SSN direction board may be contacted at http://www.ssn.unam.mx/.)

Acknowledgments

We thank the Mexican Servicio Sismológico Nacional (SSN) for providing us the data used in this work. This work was partly financed by Consejo Nacional de Ciencia y Tecnología (CONACYT) through project number 80205.

References

Ammon, C. J. (1991). The isolation of receiver effects from teleseismic *P* waveforms, *Bull. Seismol. Soc. Am.* **81,** 2504–2510.

Berteussen, K. A. (1977). Moho depth determination based on spectral ratio analysis of NORSAR long-period *P* waves, *Phys. Earth Planet. In.* **31,** 313–326.

Bertrand, E., A. Deschamps, and J. Virieux (2002). Crustal structure deduced from receiver functions via single-scattering migration, *Geophys. J. Int.* **150,** 524–541.

Campillo, M., J. C. Gariel, K. Aki, and F. J. Sanchez Sesma (1989). Destructive strong ground motion in Mexico City: Source, path and site effects during the great 1985 Michoacan earthquake, *Bull. Seismol. Soc. Am.* **79,** 1718–1735.

Campillo, M., S. K. Singh, N. Shapiro, J. Pacheco, and R. B. Herrmann (1996). Crustal structure south of the Mexican volcanic belt, based on group velocity dispersion, *Geofís. Int.* **35,** 361–370.

Cassidy, J. F. (1992). Numerical experiments in broadband receiver function analysis, *Bull. Seismol. Soc. Am.* **82,** 1453–1474.

Cruz-Atienza, V. M. (2000). Inversión global con algoritmos genéticos y cristalización simulada, aplicada a funciones de receptor: Modelos estructurales de velocidades para la corteza en la República Mexicana, *Engineering Thesis*, School of Engineering, Universidad Nacional Autónoma de México, Mexico, 215 pp.

Cruz-Atienza, V. M., J. F. Pacheco, and D. Escobedo (1998). Análisis de funciones de receptor en la parte centro-sur de la República Mexicana. Modelado inverso de las observaciones con Algoritmos Genéticos y Simulated Annealing: Estimación de la estructura cortical, *GEOS* 18**,** no. 4282–283.

Cruz-Atienza, V. M., J. F. Pacheco, S. K. Singh, N. M. Shapiro, C. Valdés, and A. Iglesias (2001). Size of Popocatépetl volcano explosions (1997–2001) from waveform inversion, *Geophys. Res. Lett.* **28,** 4027–4030.

Espíndola Castro, V. H. (2009). Modelos de velocidad cortical en México, utilizando funciones de receptor en las estaciones de la red nacional de banda ancha, *Ph.D. Thesis*, Instituto de Geofísica, Universidad Nacional Autónoma de México, Mexico, 120 pp.

Goldberg, D. E. (1989). *Genetic Algorithms in Search, Optimization and Machine Learning*. Addison Wesley Publishing Company, Reading, Massachusetts, 432 pp.

Gomberg, J. S., K. F. Priestley, T. G. Masters, and J. N. Brune (1988). The structure of the crust and upper mantle of northern Mexico, *Geophys. J.* **94,** 1–20.

Gorbatov, A., and Y. Fukao (2005). Tomographic search for missing link between the ancient Farallon subduction and the present Cocos subduction, *Geophys. J. Int.* **160,** 849–854, doi 10.1111/j.1365-246X.2005.02507.x.

Greene-Gondi, F. (2009). Geometría de la placa de Cocos usando funciones receptor a lo largo de la línea MASE, *M.Sc. Thesis*, Instituto de Geofísica, Universidad Nacional Autónoma de México, Mexico, 118 pp.

Havskov, J., and S. K. Singh (1977–78). Shallow crustal structure below Mexico City, *Geofís. Int.* **17,** 223–229.

Holland, J. H. (1975). *Adaptation in Natural and Artificial Systems*, University of Michigan Press, Ann Arbor, Michigan, 228 pp.

Husker, A., and P. Davis (2009). Tomography and thermal state of the Cocos plate subduction beneath Mexico City, *J. Geophys. Res.* **114,** no. B04306, doi 10.1029/2008JB006039.

Iglesias, A., R. W. Clayton, X. Pérez-Campos, S. K. Singh, J. F. Pacheco, D. García, and C. Valdés-González (2010). *S* wave velocity structure below central Mexico using high-resolution surface wave tomography, *J. Geophys. Res.* **115,** no. B06307, doi 10.1029/2009JB006332.

Iglesias, A., V. M. Cruz-Atienza, N. M. Shapiro, S. K. Singh, J. F. Pacheco, and S. K. Singh (2001). Crustal structure of south-central Mexico estimated from the inversion of surface-waves dispersion curves using genetic and simulated annealing algorithms, *Geofís. Int.* **40,** 181–190.

Jodicke, H., A. Jording, L. Ferrari, J. Arzate, K. Mezger, and L. Ruoke (2006). Fluid release from the subducted Cocos plate and partial melting of the crust deduced from magnetotelluric studies in southern Mexico: Implications for the generation of volcanism and subduction dynamics, *J. Geophys. Res.* **111,** no. B08102, doi 10.1029/2005JB003739.

Kirkpatrick, S., C. D. Gelatt, and M. P. Vecchi (1983). Optimization by simulated annealing, *Science* **220,** 671–680.

Langston, C. A. (1979). Structure under Mount Rainier, Washington, inferred from teleseismic body waves. *J. Geophys. Res.* **84,** 4749–4762.

Lombardi, D., J. Braunmiller, E. Kissling, and D. Giardini (2008). Moho depth and Poisson's ratio in the western–central Alps from receiver functions. *Geophys. J. Int.* **173,** 249–264, doi 10.1111/j.1365-246X.2007.03706.x.

Marsal, R. J., and R. Graue (1969). El subsuelo del lago de Texcoco, in *El Hundimiento de la Ciudad de México y Proyecto Texcoco, México, D.F.*, N. Carrillo (Editor), Secretaría de Hacienda y Crédito Público, Mexico City, Mexico 167–202.

Metropolis, N. A., A. Rosenbluth, M. Teller, and E. Teller (1953). Equation of state calculations by fast computing machines, *J. Chem. Phys.* **21,** 1087–1092.

Nieto-Samaniego, A. F., L. Ferrari, S. A. Alaniz-Álvarez, G. Labarthe-Hernández, and J. Rosas-Elguera (1999). Variation of Cenozoic extension and volcanism across the southern Sierra Madre Occidental volcanic province, Mexico, *Geol. Soc. Am. Bull.* **111,** 2–18.

Obrebski, M. J., and R. R. Castro Escamilla (2008). Seismic anisotropy in northern and central Gulf of California region, Mexico, from teleseismic receiver functions and new evidence of possible plate capture, *J. Geophys. Res.* **113,** no. B03301, doi 10.1029/2007JB005156.

Owens, T. J., G. Zandt, and S. R. Taylor (1984). Seismic evidence for an ancient rift beneath the Cumberland Plateau, Tennessee: A detailed analysis of broadband teleseismic *P* waveforms, *J. Geophys. Res.* **89,** 7783–7795.

Pérez-Campos, X., Y. H. Kim, A. Husker, P. M. Davis, R. W. Clayton, A. Iglesias, J. F. Pacheco, S. K. Singh, V. C. Manea, and M. Gurnis (2008). Horizontal subduction and truncation of the Cocos plate

beneath central Mexico, *Geophys. Res. Lett.* **35,** doi 10.1029/2008GL035127.

Persaud, P., X. Pérez-Campos, and R. W. Clayton (2007). Crustal thickness variations in the margins of the Gulf of California from receiver functions, *Geophys. J. Int.* **170,** no. 2, 687–699.

Rivet, D. N., M. Campillo, N. M. Shapiro, S. K. Singh, V. M. Cruz-Atienza, L. Quintanar, and C. Valdés (2009). Studying propagation of seismic waves across the Valley of Mexico from correlations of seismic noise, *Eos Trans. AGU* **90,** no. 52, Fall Meeting Supplement, Abstract S41C–1948.

Shapiro, N. M., M. Campillo, A. Paul, S. K. Singh, D. Jongmans, and F. J. Sánchez-Sesma (1997). Surface-waves propagation across the Mexican Volcanic Belt and the origin of long-period seismic-wave amplification in the Valley of Mexico, *Geophys. J. Int.* **128,** 151–166.

Shapiro, N. M., S. K. Singh, A. Iglesias-Mendoza, V. M. Cruz-Atienza, and J. F. Pacheco (2000). Evidence of low Q below Popocatepetl volcano, and its implication to seismic hazard in Mexico City, *Geophys. Res. Lett.* **27,** 2753–2756.

Singh, S. K., E. Mena, and R. Castro (1988). Some aspects of source characteristics of the 19 September 1985 Michoacan earthquake and ground motion amplification in and near Mexico city from the strong motion data, *Bull. Seismol. Soc. Am.* **78,** 451–477.

Urrutia-Fucugauchi, J., and J. H. Flores-Ruiz (1996). Bouguer gravity anomalies and regional crustal structure in central Mexico, *Int. Geol. Rev.* **38,** 176–194.

Valdés-Gonzáles, C., and R. P. Mayer (1996). Seismic structure between the Pacific coast and Mexico City from the Petatlán earthquake (Ms = 7.6) aftershocks, *Geofís. Int.* **35,** 377–401.

Yuan, X., S. V. Sobolev, and R. Kind (2002). Moho topography in the central Andes and its geodynamic implications, *Earth Planet. Sci. Lett.* **199,** 389–402.

Zandt, G., and C. Ammon (1995). Continental crust composition constrained by measurements of crustal Poisson's ratio, *Nature* **374,** 152–154.

Departamento de Sismología
Instituto de Geofísica
Universidad Nacional Autónoma de México
Circuito de la Investigación Científica s/n
Ciudad Universitaria
04510, México D.F.
cruz@geofisica.unam.mx
arturo@geofisica.unam.mx
krishnamex@yahoo.com
(V.M.C., A.I., S.K.S.)

Observatorio Vulcanológico y Sismológico de Costa Rica
Universidad Nacional de Costa Rica
Apartado 2346-3000
Heredia, Costa Rica
jpacheco@una.ac.cr
(J.F.P.)

Département de Sismologie
Institut de Physique du Globe de Paris
Boite 89—4 place Jussieu
75252 Paris cedex 05, France
nshapiro@ipgp.jussieu.fr
(N.M.S.)

Manuscript received 7 March 2010